



Heterogeneous TiO₂–Fe-plate catalyst for the discoloration and mineralization of aqueous solutions of cationic and anionic dyes

Haithem Bel Hadjtaief^a, Mourad Ben Zina^a, Patrick Da Costa^{b,c,*}, María Elena Gálvez^{b,c}

^aLaboratoire Eau, Energie et Environnement (LR3E), Code: AD-10-02, Ecole Nationale d'Ingénieurs de Sfax, Université de Sfax, B.P1173.W.3038, Sfax, Tunisia, emails: bel_hadj22@yahoo.com (H.B. Hadjtaief), mourad_benzina@yahoo.fr (M.B. Zina)

^bUPMC, Univ Paris 06, Sorbonne Universités, Institut Jean Le Rond d'Alembert, 2 place de la gare de ceinture, 78210 Saint Cyr L'école, France, Tel. +33 1 30 85 48 65; Fax: +33 1 30 85 48 99; emails: patrick.da_costa@upmc.fr (P. Da Costa), elena.galvez_parruca@upmc.fr (M.E. Gálvez)

^cInstitut Jean Le Rond d'Alembert, UMR CNRS 7190, 2 place de la gare de ceinture, 78210 Saint Cyr L'école, France

Received 20 February 2015; Accepted 30 May 2015

ABSTRACT

A novel structured TiO₂–Fe-plate catalyst was prepared by immobilization of iron and TiO₂ on a natural clay plate. This catalytic system allows effective mineralization of wastewaters under a wide range of operation conditions. Upon UVA irradiation and in the presence of several oxidant mixtures (H₂O₂ or/and K₂S₂O₈), this catalyst was found to be highly effective in the mineralization of malachite green and red congo in water solution. The effectiveness of this catalyst was assigned to a synergy between its photo-catalytic and photo-Fenton activities. Activity was enhanced in the presence of small amounts of K₂S₂O₈ and verified over a wide range of pH.

Keywords: TiO₂; Photocatalysis; Heterogeneous Fenton reaction; Water treatment; Dyes; Clays

1. Introduction

Synthetic dyes are extensively used in the textile industry for dyeing and coloring, as well as in cosmetics and food industries. Azo and triphenylmethane (notably, malachite green and red congo) are two of the most widely used dyes, due to their superior fastness to the applied fabric, high photolytic stability, and resistance to microbial degradation [1–3]. However, these organic compounds are toxic and potentially carcinogenic [4,5], and therefore they have to be efficiently removed from the wastewater [6].

Several physicochemical methods are currently available for the treatment of dye-colored wastewater. Chlorination has been the most widely used disinfection process. However, by-products generated are mutagenic and carcinogenic to human health [7–9]. Adsorption [10], coagulation, and flocculation methods [11–13] merely concentrate the pollutants. Sedimentation, filtration, chemical, and membrane technologies, as well as biodegradation, involve high operating costs, are not flexible to different pollutants and complete mineralization is not always achieved [4,14,15]. Advanced oxidation processes (AOPs) have positioned themselves in the last years as innovative and more effective water treatment technologies [16–18].

*Corresponding author.

Among the various AOPs, titanium dioxide (TiO₂) heterogeneous photocatalysis has recently emerged as a highly promising technology for the abatement of wastewater pollution [14,19–23]. The fundamentals and mechanism of TiO₂-photocatalysis are nowadays well known [14,21,23]. Briefly when radiation of a certain energy ($\lambda < 400$ nm) illuminates the surface of TiO₂, the electron from the valence band (VB) is excited to the conduction band (CB). This leaves an empty unfilled VB, and thus results in the creation of the so-called electron–hole pair ($h_{\text{VB}}^+ - e_{\text{CB}}^-$). The highly oxidative VB hole (h_{VB}^+) is involved in a chain of oxidation reactions, including the oxidation of organic pollutants, either directly adsorbed on the TiO₂ surface, or by means of the formation of ·OH radicals from adsorbed water. In the absence of electron scavengers, the photo-excited electron rapidly recombines with the VB hole. Therefore, the presence of electron scavengers, such as the superoxide radical O^{•2-} formed in the presence of dissolved oxygen, is crucial for avoiding this recombination and successful functioning of the photocatalyst. Other compounds that can act as electron scavengers are EDTA or t-ButOH [24] or simply H₂O₂ [25,26].

Addition of H₂O₂ will therefore boost the photocatalytic reaction. Furthermore, it will provide additional OH· radicals that will further contribute to the oxidation of the organic pollutants. Indeed, persulfate ion, S₂O₈²⁻, is a very strong oxidant which, upon thermal, photochemical, radiolytic or redox activation, generates the strange oxidant sulfate radicals, SO₄^{•-}. These radicals, together with the subsequently generated OH·, can further promote the degradation of the pollutants in the water solution. In fact, it has been claimed recently that such sulfate radicals are more selective for oxidizing unsaturated bond and aromatic constituents [27]. Furthermore, a synergetic effect between SO₄^{•-} and OH· radicals has been observed upon the addition of small amounts of K₂S₂O₈, in the photo-oxidation of pharmaceutical compounds [28] and organic surfactants [29].

The addition of H₂O₂ as electron scavenger and oxidant, mixed or not with other reagents such as S₂O₈²⁻, can be moreover combined with the presence of Fe-compounds, in order to further increase the degradation efficiency of water pollutants [29]. In fact, the photo-Fenton process remains one of the most applied AOPs for the degradation of organic water pollutants [17,30–33]. Several works published in the last decade show evidences of this synergy when combining both AOPs, i.e. photocatalysis-photo-Fenton for the degradation of oxalic acid [31], Methylene blue, reactive black, and acid red dyes [34], ultrasound-assisted mineralization of bisphenol [35], or basic red

dye via the combination of photoelectron-Fenton and photocatalysis [36].

Still, one of the fundamental technical challenges of photocatalysis remains the post-separation of the TiO₂ catalyst after water treatment. In a similar way, homogeneous Fenton processes suffer from the serious drawback of iron recuperation from the stream of treated water. TiO₂-nanoparticles, as well as Fe compounds [37–39], can be immobilized in a wide range of materials, such as carbon materials [40–42], thin films [43], silicas [44], zeolites [29,45,46], or clays [30,31,47,48]. The use of clays represents in fact a promising alternative since they are natural, abundant, inexpensive, and environmentally friendly. However, the reutilization of all these generally powder-structured catalysts still implies the filtration or decantation of the water treated, which will considerably increase the overall process cost. In this sense, the challenge lies in the preparation of structured and active catalytic systems for water treatment which will bypass this filtration step.

In a previous paper, we presented a novel structured photo-Fenton plate catalyst prepared by immobilizing iron species on the surface of natural Tunisian clay [49]. This plate-catalyst represents a low cost, easy to fabricate option for water treatment. Moreover, it showed to be highly efficient in the photo-Fenton reaction for total oxidation of phenol. However, phenol removal efficiency was found to decrease when using radiation wavelengths in the UVA range (365 nm), with respect to UVC irradiation (245 nm). In the present work, we aimed to combine the outstanding activity of the plate Fe-catalyst in the photo-Fenton process, with a photocatalytic active compound, such as TiO₂, for extending its range of application to wavelengths in the UVA range, closer to the visible spectra. In this sense, both Fe and TiO₂ were immobilized on the surface of natural clay plate. The activity of the catalyst was assayed in the combined photocatalytic-photo-Fenton reaction for the mineralization of two azo dyes: malachite green (MG) and red congo (RC). Discoloration and mineralization of these organic compounds are discussed, considering also the addition of small amounts of S₂O₈²⁻ as a stronger oxidizing agent. The effects of operational parameters, such as initial dye concentration, initial solution pH, and reaction temperature, are as well evaluated.

2. Materials and methods

2.1. Preparation of the TiO₂–Fe-plate catalyst

Natural clay from Jebel Tejera–EsgHIRA, 9 km north-east the Medenine area (southeast of Tunisia), was

used as a raw material. The procedures for purification and preparation of the saturated sodium form of similar natural clays have been described in detail in previous works [46,47].

For the preparation of the plates, the natural clay was combined with water and sand (clay/sand weight ratio of 1:1). The mix was molded forming circular plates (7.8 cm diameter, 0.4 cm thickness), which were dried controllably at 25°C for 24 h, in order to avoid the formation of fissures. Finally, the dried plate was calcined at 250°C for 4 h.

Before Fe and TiO₂ loading, the plate was treated with a HNO₃ solution (10 wt.%) at room temperature for 18 h. For its impregnation with the iron compounds, the plate was immersed in 100 mL of a 2 g L⁻¹ aqueous solution of Fe(III) (Fe(NO₃)₃·9H₂O, 97% purity, Sigma-Aldrich) at pH ca. 2.0, and then kept at 48°C for 2 h under continuous magnetic stirring. The plate was removed from the solution, carefully washed, and immersed again for a total of three consecutive cycles of impregnation. The Fe-loaded plate was dried at 25°C for 24 h and subsequently calcined at 350°C for 2 h.

For the deposition of the titanium oxide coat, the Fe-loaded plate was immersed in 30 mL of a solution of titanium tetraisopropoxide at 100°C (98% purity, Sigma-Aldrich), and kept under vigorous stirring for 3 h. Subsequently, the TiO₂-Fe-plate was removed from the solution, carefully washed with distilled water, and finally calcined at 450°C for 4 h. Fig. 1(a) shows a picture of this TiO₂-Fe-plate catalyst.

2.2. Characterization of TiO₂-Fe-plate

The chemical composition and structural features of the natural clay were analyzed by means of X-ray fluorescence (XRF, ARL[®] 9800 XP spectrometer), powder X-ray diffraction (XRD Philips[®] PW 1710 diffractometer, K α , 40 kV/40 mA, with a scanning rate of 2 θ per min) and infrared spectroscopy (IR, Digilab Excalibur

FTS 3000 spectrometer). BET surface areas and pore volumes of the solids were determined by nitrogen adsorption at -196°C (Micrometitics ASAP 2010).

The morphology of plates was studied using scanning electronic microscopy (SEM, Hitachi SU-70). This equipment has an Oxford X-Max 50 mm² X-ray spectroscopy system through dispersive energy (EDX), which enabled qualitative evaluation of chemical composition. High resolution transmission electron microscopy images were acquired on a JEOL JEM 2011 equipped with LaB₆ filament and operating at 200 kV. The images were collected with a 4,008 × 2,672 pixel CCD camera (Gatan Orius SC1000) coupled with the DIGITAL MICROGRAPH software. Chemical analyses were obtained by an EDX microanalyzer (PGT IMIX PC) mounted on the microscope. The plates were grinded, dispersed in ethanol, and sonicated. A drop of the dispersion was deposited on a carbon-coated copper grid for the TEM observations.

2.3. Activity tests

The photo-catalytic experiments were carried out in a 500 mL double-glass cylindrical jacket reactor filled with 200 mL of aqueous dye solution. This double-glass cylindrical jacket permitted the constant circulation of water, allowing an accurate control of the temperature in reaction solution within $\pm 0.5^\circ\text{C}$. The plate catalyst was immersed into the 200 mL dye solution and kept under continuous stirring. The radiation source used was a 100 watt UV lamp (type Black-Ray B 100AP UV 230 V–50 Hz/2.0 Amps), with maximum emission at 365 nm. The distance between the solution and the UV source was kept constant at 15 cm. A schematic representation of this experimental installation is presented in Fig. 1(b).

In the activity tests, different aqueous solutions of malachite green (cationic, MG, C.I. 42000, chemical formula C₂₃H₂₅N₂Cl, FW = 364.91 g/mol, Sigma-Aldrich), and red congo (anionic, RC, C.I.

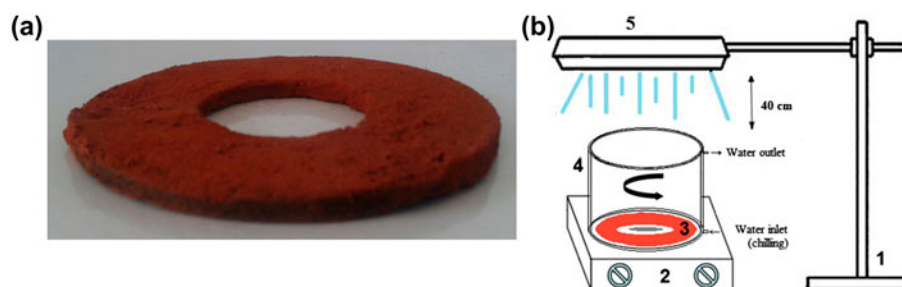


Fig. 1. (a) Picture of the TiO₂-Fe-plate catalyst and (b) experimental setup (1: support, 2: magnetic stirrer, 3: plate, 4: open Pyrex reactor, 5: UV lamp, $\lambda = 365$ nm).

22120, chemical formula $C_{32}H_{22}N_6Na_2O_6S_2$, FW = 696.7 g/mol, Sigma-Aldrich) were used. The experiments were performed at natural pH of 4.25 for MG, 7.32 for RC, and 4.44 for the mixtures RC/MG, except when noted. Either hydrogen peroxide (H_2O_2 , 35% conc., MERCK), potassium peroxydisulfate ($K_2S_2O_8$, 98% purity, MERCK), or their different mixtures, were added to the dye solution. UV-light was turned on right after the addition of the oxidizing agents.

The analysis of the concentration of the dyes in the solution was performed by periodically withdrawing aliquots of 2 mL from the reactor. Concentration of MG and RC was then measured by means of UV-vis spectrophotometer (Shimadzu 2450, Japan) and in a total organic carbon, TOC, analyzer (Shimadzu TOC-5000A, Japan). Before analysis, samples were filtered through a 0.45 μm membrane filter and a scavenging agent (0.1 M Na_2SO_3 , 0.1 M KH_2PO_4 , 0.1 M KI, and 0.05 M NaOH) was added, in order to stop all possible oxidation reactions. Note that typical UV-vis spectra for MG present two absorption peaks at 618 and 425 nm, ascribed to its extended chromophore, and a third absorption band at 315, due to the benzene ring structure of the dye molecule [50]. In the case of RC, peaks appear at 499 nm corresponding to the azo bonds, and at 236 and 345 nm attributed to the benzene and naphthalene rings, respectively [51]. The absorption peaks at 618 and 499 nm were used to monitor the discoloration of MG and RC, respectively.

Discoloration efficiency and mineralization efficiency were calculated as follows:

$$\eta (\%) = \frac{C_0 - C_t}{C_0} \times 100 \quad (1)$$

where C_t and C_0 denote to the time-dependent concentration/TOC and the initial concentration/TOC, respectively.

3. Results and discussion

3.1. Physicochemical characterization

The chemical composition of the natural clay, as analyzed by means of XRF, has been presented elsewhere [49]. Briefly, its main constituents are silica, alumina, iron, and calcium. The relatively high iron content in the natural clay (17.5 wt.% Fe_2O_3) is a common feature among in Tunisian clays [50]. XRD evidenced that quartz, kaolinite, and illite are the main crystalline phases [49]. The analysis of the N_2 adsorption isotherm acquired for this raw clay yielded a

value of BET surface area of $37 \text{ m}^2 \text{ g}^{-1}$, and a total pore volume of $0.13 \text{ cm}^3 \text{ g}^{-1}$, being composed mostly of pores in the range of wide mesopores and macropores. The XRD patterns for the TiO_2 impregnated plates evidence a dominant presence of anatase (around 95%).

Morphological observations by SEM reveal that surface morphology of the raw clay is different from the TiO_2 -Fe-modified one (Fig. 2). The clay is observed as dense sheets and flake-like crystal with fluffy appearance, revealing its extremely fine platy structure. After impregnation with the Fe-compounds and TiO_2 , the clay becomes more porous and fluffy. SEM-EDX analysis evidenced increased content of Fe and presence of Ti in the clay after impregnation.

Further insight on the structural and morphological changes occurring after impregnation of the clay was gained through TEM analysis of these materials, concretely in terms of the different crystalline and amorphous phases that can be distinguished by TEM, moreover when coupled to EDS analysis. Fig. 3 shows the TEM images acquired for both a Fe-impregnated clay and the Fe- TiO_2 -plate. Though not shown in Fig. 3(a), Fe crystallites of very different sizes were found in the observation of the Fe-plate catalyst. The platy structure of the clay can be still perfectly observed in Fig. 3(a). However, upon TiO_2 loading, Fig. 3(b), clay is considerably covered by this new phase, which possesses clearly a different morphology. EDS analysis confirmed the coexistence of Fe and TiO_2 , pointing to a successful impregnation of the clay plate (Fig. 3(c) and (d)).

3.2. MG and RC oxidation

Fig. 4(a) and (b) shows the discoloration efficiency measured as a function of reaction/irradiation time for MG and RC solutions, both in the presence or in absence of the Fe- TiO_2 -plate and/or H_2O_2 and UV-irradiation. Fig. 4(a) and (b) contain as well the results of the discoloration experiments in the presence of the analogous catalyst prepared only by impregnation of the clay with the Fe compounds, i.e. in absence of TiO_2 . For both discoloration of MG and RC solutions, the Fe- TiO_2 -plate itself shows a certain activity, around 10%, even in absence of radiation and of any oxidant. Not surprisingly, this was observed before for a Fe-pillared clay catalyst [48], and could be most probably due to the adsorption of dye molecules on the catalyst surface, more than to real catalytic degradation. Experiments were also performed in absence of the Fe- TiO_2 -plate, just in the presence of H_2O_2 and under UV irradiation. Considerable

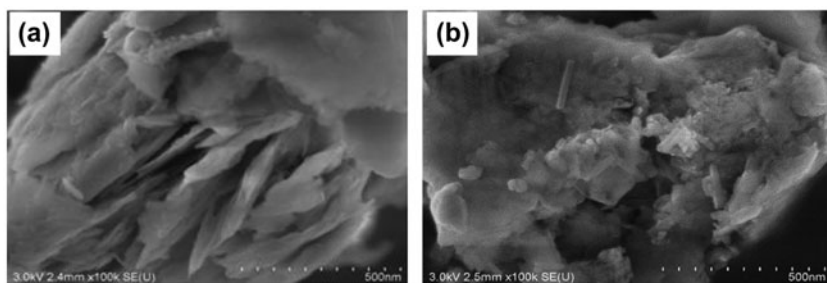


Fig. 2. SEM images for (a) raw clay and (b) TiO₂-Fe-plate.

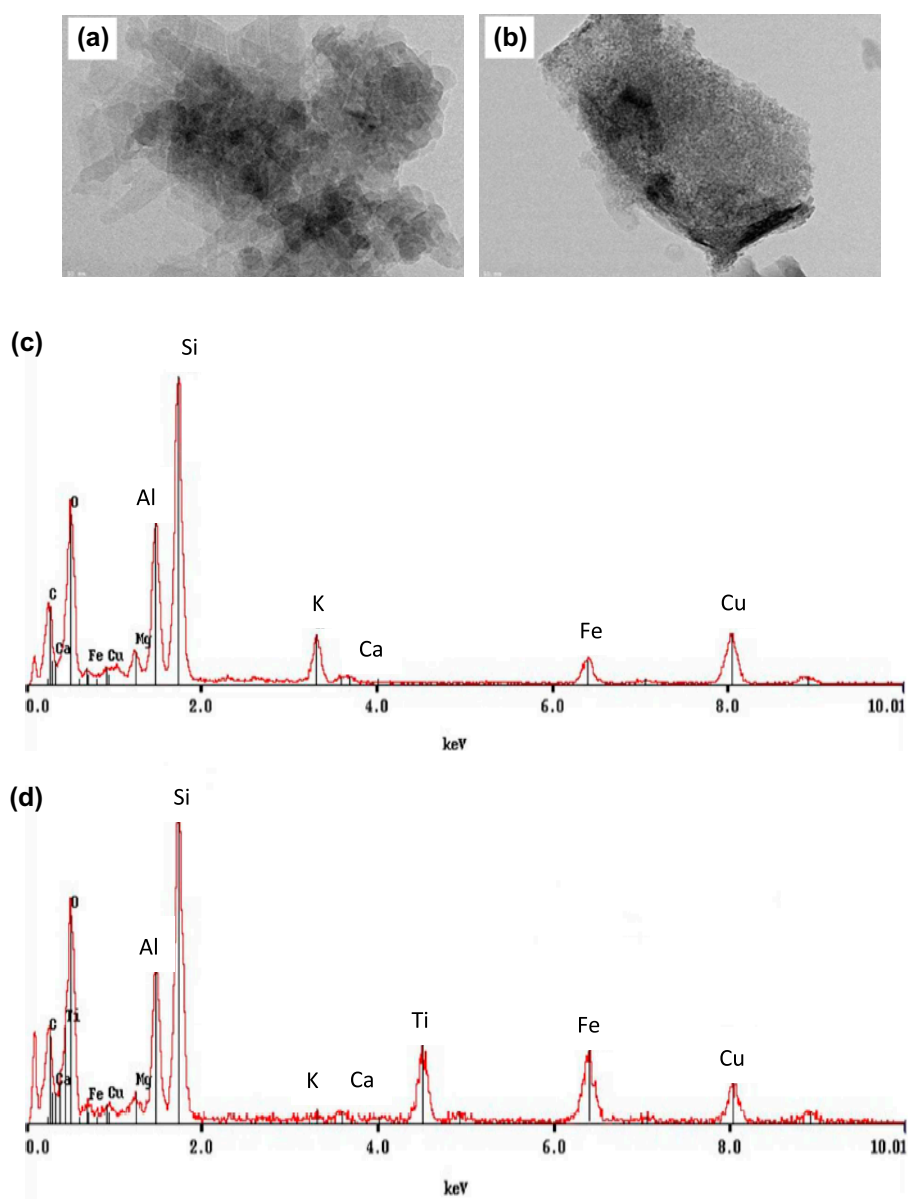


Fig. 3. TEM images for (a) raw clay, (b) TiO₂-Fe-plate, and EDS measurements for (c) raw clay, and (d) TiO₂-Fe-plate.

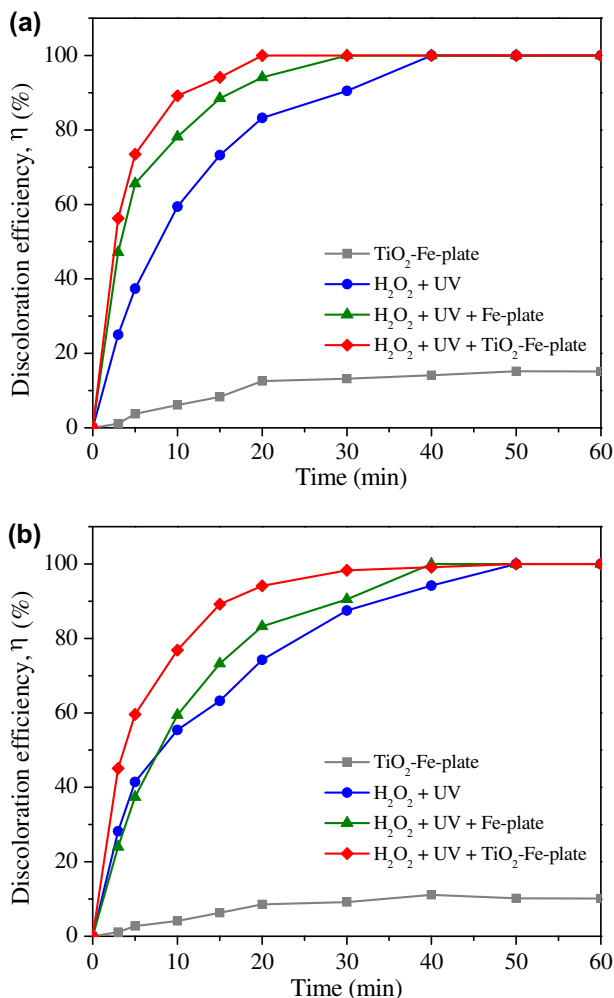


Fig. 4. Discoloration efficiency as a function of reaction time, under different catalytic systems and reaction conditions for (a) MG and (b) RC.

discoloration efficiency was measured in this case for both MG and RC solutions. However, rate of discoloration increases notably already when the Fe-plate catalyst is present, and moreover when the Fe-TiO₂-plate is used. This points first to a catalytic effect due to the presence of Fe, due to the activation of a Fenton-type process promoting the degradation of dye molecules that is furthermore enhanced when TiO₂ is present in the catalyst formulation. Full discoloration of the solution is reached after 20 min irradiation in the case of MG and after 30 min irradiation for RC, around 10 min earlier when using the Fe-TiO₂-plate than when using the non-TiO₂ containing catalyst, Fe-plate. The positive influence in the presence of TiO₂ is thus proven, especially under the wavelengths used in this study, i.e. UVA range (365 nm). Let us remark here the already observed more difficult

oxidation of RC, a diazo dye, in comparison to MG [48]. Full discoloration of the solution is more readily achieved for MG than for RC, this easiness of degradation being due to its lower molecular weight and less complex chemical structure.

Fig. 5 shows the discoloration efficiency measured using different combinations of the two oxidizing agents considered in this work, H₂O₂ and K₂S₂O₈, for both MG and RC containing solutions. The oxidizing power of K₂S₂O₈ is demonstrated even in absence of catalyst and upon the addition of relatively very small quantities, exactly 0.046 mmol/L. Moreover, as could be expected, oxidation capacity is boosted in the presence of the Fe-TiO₂-plate. However, right choice of oxidizing agent results in similar activity for lower total amount of oxidant used. In example, comparing the discoloration efficiency curves determined for both

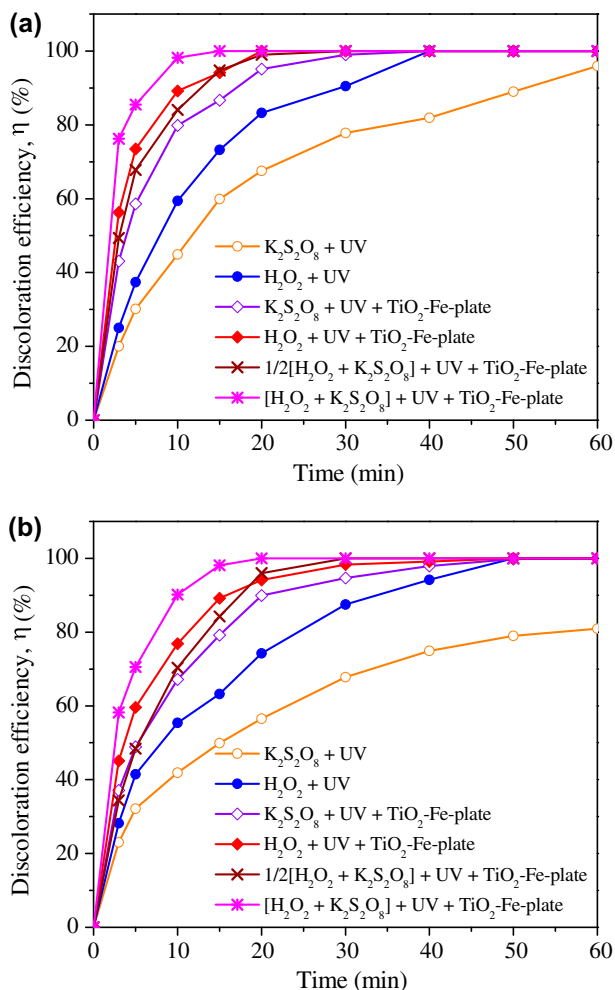


Fig. 5. Discoloration efficiency in the presence of the TiO₂-Fe-plate, using different oxidants and mixtures for (a) MG and (b) RC.

RC and MG solutions, in the presence of the Fe–TiO₂-plate, using either 0.368 mmol/L H₂O₂ and the combination 1/2[H₂O₂ + K₂S₂O₈], corresponding to 0.184 mmol/L H₂O₂ + 0.023 mmol/L K₂S₂O₈, that is 0.207 mmol/L total concentration of oxidant, both follow a similar path, reaching 100% discoloration efficiency after almost the same irradiation time (20 min for MG, 30 min for RC). Of course, further increasing the concentration of oxidants, [H₂O₂ + K₂S₂O₈] = 0.414 mmol/L, allows faster reaction, with full discoloration being achieved after roughly 10 min irradiation time for the MG solution and after 20 min for the RC containing one.

These results prove the enhancement of the degradation of organic molecules when adding small amounts of the stronger oxidant S₂O₈²⁻, in agreement with previously published literature [27,28,52], and point to the importance of correctly choosing the amount and combination of the two different oxidants considered. Note, however, that in the works presented by Saien et al. and Chu et al. larger amounts of oxidants were employed, and, more importantly, pH was adjusted to 3–4, whereas in the present study reaction was studied at natural solution pH (4.25 and 7.32 for MG and RC solutions, respectively).

Experimental data were fitted to a pseudo-first-order kinetic model: $\ln C_0/C = kt$. Fig. 6 shows the different plots $\ln C_0/C$ vs. t obtained. The linearity of these plots confirms the adequacy of using such a pseudo-first-order kinetic model. The slope represents the apparent kinetic constant for the decolorization of MG and RC. The values obtained for these constants are presented in Table 1. The apparent kinetics constant calculated after 15 min irradiation time are only slightly lower for the discoloration experiments using (0.184 mmol/L + 0.023 mmol/L) 1/2[H₂O₂ + K₂S₂O₈], than for the experiment only using 0.368 mmol/L H₂O₂. Obviously, doubling the concentration of the oxidant mixture [H₂O₂ + K₂S₂O₈] results in higher values of the apparent kinetic constant and a faster discoloration of both MG and RC solutions.

Fig. 7 shows the mineralization efficiency calculated from TOC measurements at different irradiation times, for several concentration of MG and RC and their mixtures, using the oxidant combination [H₂O₂ + K₂S₂O₈], and in the presence of the Fe–TiO₂-plate. As expected, comparing the results presented in Figs. 4 and 5, in terms of discoloration efficiency, to the mineralization efficiencies measured at the same irradiation time, Fig. 7, it becomes clear that discoloration, i.e. destruction of the chromophore of the dye, takes place more readily than

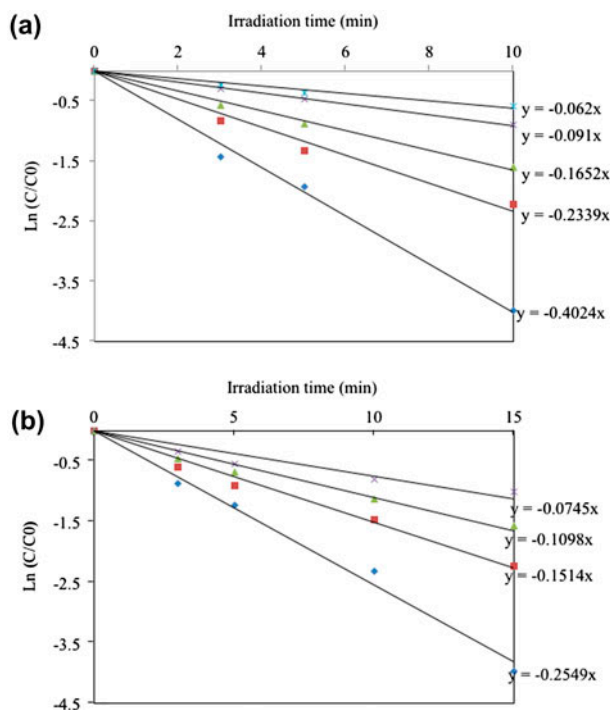


Fig. 6. $\ln C_0/C$ vs. t plots for the degradation of MG and RC dyes.

the total mineralization of the organic compounds. Total oxidation of the dye thus occurs stepwise, through the formation of intermediate and more refractory species that are subsequently oxidized to CO₂. However, 100% mineralization is achieved after 40 min irradiation time, for both 25 m/L solutions of either MG or RC. Mineralization is faster though for MG and RC. This fact becomes even more remarkable when increasing the concentration of dye in the initial solution. In example, for a solution containing 50 mg/L RC, complete mineralization occurs only after 60 min time on stream. The mixture 25 mg/L MG and 25 mg/L RC is mineralized at an intermediate rate. Increased chemical complexity and molecular weight of the dye, as well as increased dye concentration, result, as expected, in a more difficult and slower degradation that may require longer irradiation times. This fact may due to a higher occupation of the active sites on the surface of the catalyst by adsorbed dye molecules, and to a higher adsorption of photons by the dye molecules, which will hinder the photo-oxidation reaction [48,53–55]. Finally, it is important to notice that after several runs of experiments the amounts of Fe or derivate products coming from the plate are negligible in solution.

Table 1

Discoloration efficiency measured and apparent kinetic constant (pseudo-first-order kinetics) determined after 15 min irradiation time, for both MG and RC solutions, using different concentrations and mixtures of the two oxidizing agents

Activity test	MG solution			RC solution		
	η (%)	K_{app} (s ⁻¹)	R^2	η (%)	K_{app} (s ⁻¹)	R^2
(0.046 mmol/L) K ₂ S ₂ O ₈ + UV + TiO ₂ -Fe-plate	79.9	0.165	0.99	67.2	0.109	0.97
(0.368 mmol/L) H ₂ O ₂ + UV + TiO ₂ -Fe-plate	89.2	0.233	0.98	76.9	0.159	0.98
(0.184 mmol/L + 0.023 mmol/L) 1/2[H ₂ O ₂ + K ₂ S ₂ O ₈] + UV + TiO ₂ -Fe-plate	94.7	0.196	0.99	84.2	0.123	0.99
(0.368 mmol/L + 0.046 mmol/L) [H ₂ O ₂ + K ₂ S ₂ O ₈] + UV + TiO ₂ -Fe-plate	98.2	0.402	0.99	90.6	0.254	0.99

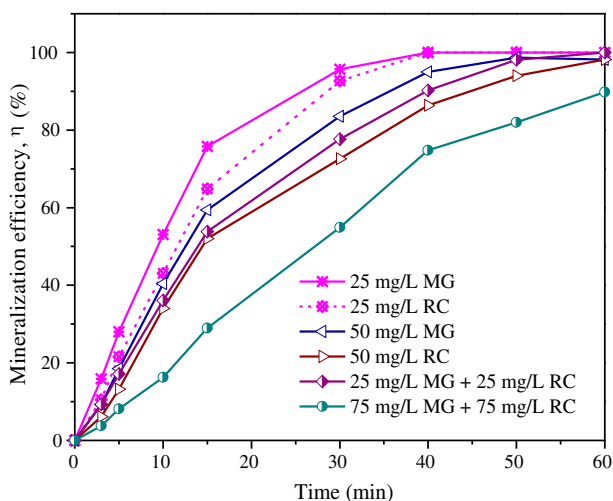


Fig. 7. Mineralization efficiency (TOC) as a function of irradiation time for different initial dye concentration and their mixtures.

3.3. Effect of operating conditions

3.3.1. Influence of initial pH

Due to the wide range of pH of industrial wastewaters and the influence of this parameter on the catalytic activity and stability of water-treatment catalysts, pH value is an important factor in the assessment of photo-catalytic and Fenton processes. Ideally, the catalytic system used in such applications should be able to work steadily over a wide range of pH, without any adjustment of solution pH.

Fig. 8 shows the mineralization efficiency measured at different initial pH, during the degradation of a solution containing 25 mg/L of MG and 25 mg/L of RC, using the oxidant combination [H₂O₂ + K₂S₂O₈], and in the presence of the Fe-TiO₂-plate. The dashed line shows the mineralization efficiency measured after 30 min irradiation time, whereas the solid line displays the values of mineralization efficiency

recorded after 60 min irradiation time. Six different pH values were assayed: 2.5, 4.44 (natural pH of the MG-RC solution), 5.75, 7.94, 9.11, and 11.24, and pH was adjusted using high concentration solutions of either HCl or NaOH. The results presented in Fig. 8 evidence that upon 60 min irradiation time, complete mineralization of the dyes can be achieved over a wide range of pH, i.e. between 2.5 and 7.94. Of course, the mineralization efficiency measured only after 30 min irradiation time is much lower than that registered after 60 min, but the curve follows the same trend.

This extended range of pH solves one of the critical drawbacks of the typical homogeneous Fenton system, i.e. active only under highly acidic conditions pH 2–3 [56]. When using pillared clays as catalysts, it has been nevertheless reported that this problem can be solved through a modification of the pillaring method [57,58], pointing already to a significant advantage of using such heterogeneous catalysts for Fenton oxidation processes. The reason for the good photocatalytic

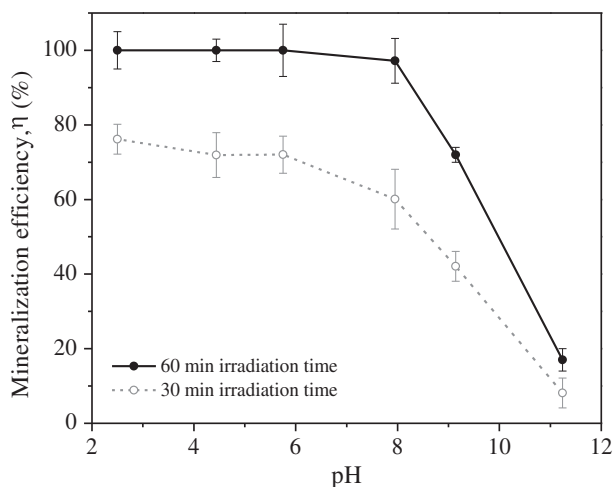


Fig. 8. Influence of pH on the mineralization efficiency of a mixture of MG and RC dyes.

activity of these materials when the initial pH of the solution is 6.6–7.0 has been attributed before to a decrease of the pH occurring along the oxidation, due to the formation of acidic intermediates such as muconic, maleic or oxalic acids [59,60]. Najjar and co-workers and Catrinescu et al. stated that due to the specific environment of ferric species in Fe-pillars, active iron species can exist even at neutral pH and they can establish an effective Fenton-type redox system [57,59]. In fact, some other authors claim that in heterogeneous systems, the immobilized Fe(III) species are not easily transformed into less photoactive materials, i.e. $[\text{Fe}(\text{H}_2\text{O})_6]^{3+}$ at lower pH and $\text{Fe}(\text{OH})_3$ at higher pH [61]. In this sense, the interaction of the clay matrix with the Fe-compounds results in a stabilization of the active phase, this interaction probably being enhanced in our case, as a consequence of the impregnation-type preparation method instead of pillaring, but also to the presence of TiO_2 .

3.3.2. Influence of temperature

The influence of temperature on the photocatalytic-photo-Fenton degradation of MG and RC dyes in the presence of the Fe– TiO_2 -plate was investigated, using an initial mixture of 75 mg/L MG and 75 mg/L RC, and the oxidant combination $[\text{H}_2\text{O}_2 + \text{K}_2\text{S}_2\text{O}_8]$, at natural solution pH. TOC removal was measured at 25, 30, and 40 °C after 60 min irradiation time. Results are presented in Fig. 9. TOC removal, i.e. mineralization efficiency, increases significantly with reaction temperature. Mineralization efficiency increases from 89% at 25 °C to 98% at 30 °C, and reaches 100% at 40 °C. This trend is in complete agreement to what has been previously reported, for the photo-catalytic oxidation of various organic compounds [28,55,62].

The apparent kinetic constant values, k_{app} , were calculated considering:

$$\ln \text{TOC}_t = -k_{\text{app}} \cdot t + \ln \text{TOC}_0 \quad (2)$$

where TOC_t and TOC_0 are the TOC measured at a time t and the initially present in the dye mixture. We can assume as well that k_{app} follows an Arrhenius-type dependency with temperature, thus:

$$\ln k_{\text{app}} = \ln A - \frac{E_a}{R} \frac{1}{T} \quad (3)$$

where A is the pre-exponential factor and E_a the activation energy of the degradation reaction, T is the absolute temperature in K, and R is the universal gas constant. The value of the apparent activation energy

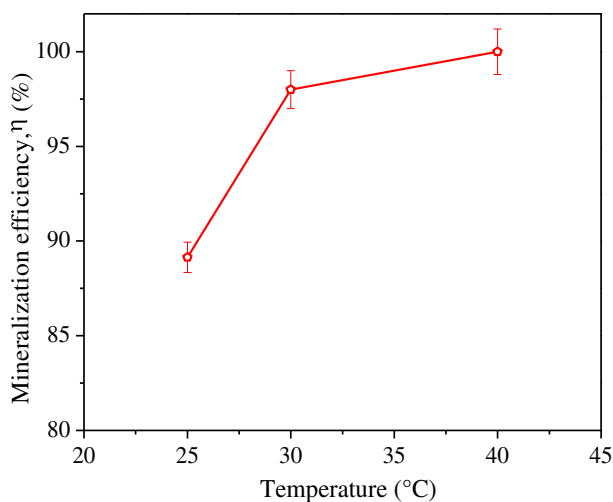


Fig. 9. Influence of temperature on the mineralization efficiency of a mixture of MG and RC dyes.

estimated from the linear regression of Eq. (3) was found to be $E_a = 56.9 \text{ kJ mol}^{-1}$. This value is slightly higher than the one we reported in a previous work for a Fe-plate catalyst, i.e. 48.7 kJ mol^{-1} . However, UVC irradiation (245 nm) was used instead of UVA radiation (365 nm), which was the one in fact employed in the present work.

Moreover, the activation enthalpy and the entropy for the degradation reaction can be calculated by means of the Eyring equation in its thermodynamic formulation:

$$k_{\text{app}} = \frac{k_B T}{h} \exp\left(-\frac{\Delta H^*}{RT}\right) \exp\left(\frac{\Delta S^*}{R}\right) \quad (4)$$

where ΔH^* is the activation enthalpy, ΔS^* the activation entropy, k_B is the Boltzmann constant, h is the Planck constant. The linearization of this equation leads to:

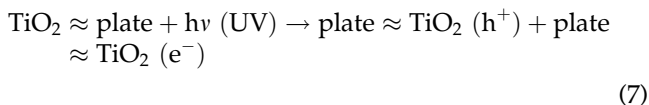
$$\ln \frac{k_{\text{app}}}{T} = \ln\left(\frac{k_B}{h}\right) + \frac{\Delta S^*}{R} - \frac{\Delta H^*}{R} \frac{1}{T} = \text{const.} - \frac{\Delta H^*}{R} \frac{1}{T} \quad (5)$$

Therefore, the different thermodynamic parameters can be extracted by means of a simple linear regression. Enthalpy and entropy values obtained were: $\Delta H^* = 48.2 \text{ kJ mol}^{-1}$ and $\Delta S^* = -0.241 \times 10^{-3} \text{ kJ mol}^{-1}$. The value of $\Delta H^* > 0$ is clearly indicative of the endothermic nature of the degradation process. The negative value of ΔS^* may imply a certain rigidity of the reacting dyes molecules, so that they react only in given reduced number of states or geometrical orientations. Therefore, the high efficiency of the TiO_2 -Fe-plate

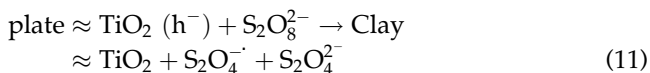
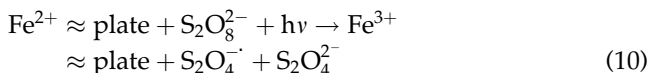
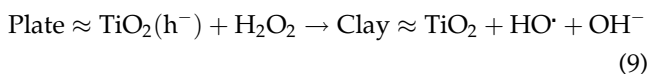
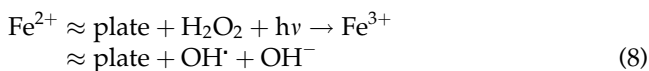
catalyst in this oxidation could be explained by the formation of an activated complex of such adsorbed molecules on the catalyst surface. In fact, as already discussed in previous sections, adsorption of the organic compounds was always observed during the runs in the sole presence of the plate catalyst.

On the basis of the existing literature and in agreement with the experimental results obtained, the following mechanism for the degradation of MG and RC dyes can be proposed:

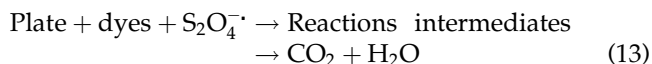
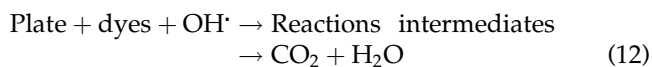
- (1) Dye molecules are first adsorbed on the surface of the plate (\approx)
- (2) Under UV irradiation, the photo-reduction of Fe^{3+} on the surface of the TiO_2 -Fe-plate to Fe^{2+} follows Eq. (6). The photoexcitation with UV irradiation having an energy greater than the TiO_2 band gap promotes an electron from the VB to the conduction band, and leaves an electronic vacancy or hole (h^+) in the VB. Photoexcitation generates thus an electron-hole pair (Eq. (7)):



- (3) Hydroxyl (OH^\cdot) and sulfate ($\text{SO}_4^{\cdot-}$) radicals are formed through reaction at the clay surface (Eqs. (8) and (9)) for hydrogen peroxide and Eqs. (10) and (11) for the persulfate):



- (4) Hydroxyl radicals can finally attack the organic molecules adsorbed on the surface of the catalyst leading to its degradation (Eqs. (12) and (13)):



The possibility of reusing the photocatalyst was examined through subsequent utilization of the Fe-TiO₂-plate. After each use the catalyst was separated, thoroughly washed with distilled water, and reused for subsequent reaction using a fresh dye solution. The catalyst can be used for at least five times maintaining mineralization efficiency higher than 90%. ICP-OES analysis confirmed the absence of Ti or Fe ions in the treated solutions.

4. Conclusions

A local Tunisian clay was used for the preparation of a novel clay-plate structured catalyst, containing iron compounds and TiO₂ as the active phase. Its activity was assayed in the degradation of MG and RC dyes, under UVA irradiation (365 nm), and using either H₂O₂ and K₂S₂O₈ or their mixtures as oxidants. Such a catalytic system will allow effective water treatment under a wide range of conditions and for different pollutants and their mixtures, at low cost, and by-passing the need for a separation/filtration step to recover the catalyst.

With respect to a similar catalyst only containing the iron compounds, the TiO₂-containing catalyst, TiO₂-Fe-plate, showed enhanced ability toward the degradation of both MG and RC. This fact was assigned to the combination and positive synergy of both the photo-catalytic and photo-Fenton activity in the TiO₂-Fe-plate. Addition of a small amount of K₂S₂O₈ to H₂O₂ resulted in a powerful combination of oxidants, further enhancing the degradation of the dyes, which in turn was found to follow pseudo-first-order kinetics. As expected, total mineralization of the dyes followed the initial discoloration of the dye solutions, which is just a consequence of the destruction of their chromophore, with oxidation of RC being all the time more sluggish than that of MG.

The TiO₂-Fe-plate catalyst was found to efficiently oxidize MG and RC over quite a wide range of pH, and is a stable material with time on stream pointing to an important advantage of using such heterogeneous systems, i.e. vis-à-vis the classical homogeneous Fenton process. Temperature was found to strongly influence the endothermic dye degradation reaction,

which was found to depend as well of an initial adsorption step for the activation of dye molecules on the catalyst surface.

References

- [1] Q.Y. Xiu, X.Z. Xiao, Y.L. Cheng, Z. Yuan, J.Q. Shi, Decolorization of azo, triphenylmethane and anthraquinone dyes by a newly isolated *Trametes* sp. SQ01 and its laccase, *Process Biochem.* 44 (2009) 1185–1189.
- [2] Z. Yang, B. Gao, Y. Wang, X. Liu, Q. Yue, Y.W. Shu, Synthesis and application of polyferric chloride-poly (epichlorohydrin-dimethylamine) composites using different crosslinkers, *Chem. Eng. J.* 213 (2012) 8–15.
- [3] H. Zollinger, *Colour Chemistry Synthesis Properties and Applications of Organic Dyes and Pigments*, VCH Publishers, New York, NY, 1987.
- [4] L.N. Du, Z. Ming, L. Gang, C.X. Fang, H.C. Wen, H.Z. Yu, Biodegradation of malachite green by *Micrococcus* sp. strain BD15: Biodegradation pathway and enzyme analysis. *Int. Biodeterior. Biodegrad.* 78 (2013) 108–116.
- [5] M.D. Murcia, M. Gómez, E. Gómez, J.L. Gómez, N. Christofi, Photodegradation of congo red using XeBr, KrCl and Cl₂ barrier discharge excilamps: A kinetics study, *Desalination* 281 (2011) 364–371.
- [6] K. Rajeshwar, M.E. Osugi, W. Chanmanee, C.R. Chenthamarakshan, M.V.B. Zanoni, P. Kajitvichyanukul, R. Krishnan-Ayer, Heterogeneous photocatalytic treatment of organic dyes in air and aqueous media, *J. Photochem. Photobiol. C: Photochem. Rev.* 9 (2008) 171–192.
- [7] H. Yang, H. Cheng, Controlling nitrite level in drinking water by chlorination and chloramination, *Sep. Purif. Technol.* 56 (2007) 392–396.
- [8] J. Lu, T. Zhang, J. Ma, Z. Chen, Evaluation of disinfection by-products formation during chlorination and chloramination of dissolved natural organic matter fractions isolated from a filtered river water, *J. Hazard. Mater.* 162 (2009) 140–145.
- [9] H.M. Coleman, C.P. Marquis, J.A. Scott, S.S. Chin, R. Amal, Bactericidal effects of titanium dioxide-based photocatalysts, *Chem. Eng. J.* 113 (2005) 55–63.
- [10] O. Abdil, C.S. Keskin, Removal of a binary dye mixture of congo red and malachite green from aqueous solutions using a bentonite adsorbent, *Clays Clay Miner.* 57 (2009) 695–705.
- [11] N.A. Oladoja, Y.D. Aliu, Snail shell as coagulant aid in the alum precipitation of malachite green from aqua system, *J. Hazard. Mater.* 164 (2009) 1496–1502.
- [12] P. Himanshu, R.T. Vashi, Removal of Congo Red dye from its aqueous solution using natural coagulants, *J. Saudi Chem. Soc.* 16 (2012) 131–136.
- [13] P.V.A. Padmanabhan, K.P. Sreekumar, T.K. Thiyagarajan, R.U. Satpute, K. Bhanumurthy, P. Sengupta, G.K.K. Dey, G.K. Warriar, Nano-crystalline titanium dioxide formed by reactive plasma synthesis, *Vacuum* 80 (2006) 11–12.
- [14] U.I. Gaya, A.H. Abdullah, Heterogeneous photocatalytic degradation of organic contaminants over titanium dioxide: A review of fundamentals, progress and problems, *J. Photochem. Photobiol. C: Photochem. Rev.* 9 (2008) 1–12.
- [15] K.P. Gopinath, S. Murugesan, J. Abraham, K. Muthukumar, *Bacillus* sp. mutant for improved biodegradation of Congo red: Random mutagenesis approach, *Bioresour. Technol.* 100 (2009) 6295–6300.
- [16] S. Esplugas, J. Giménez, S. Contreras, E. Pascual Rodriguez, Comparison of different advanced oxidation processes for phenol degradation, *Water Res.* 36 (2002) 1034–1042.
- [17] M. Pera-Titus, V. García-Molina Baños, J. Gimenez, S. Esplugas, Degradation of chlorophenols by means of advanced oxidation processes: A general review, *Appl. Catal. B: Environ.* 47 (2004) 219–256.
- [18] S.J. Yong, T.L. Woo, J.-Y. Park, Y.-H. Kim, Effect of pH on Fenton and Fenton-like oxidation, *J. Environ. Technol.* 30 (2009) 183–190.
- [19] C.-Y. Kuo, C.-H. Wu, S.-T. Chen, Decolorization of C.I. Reactive Red 2 by UV/TiO₂/PAC and visible light/TiO₂/PAC systems, *J. Desalin. Water Treat.* 52 (2014) 834–843.
- [20] K. Nakata, A. Fujishima, TiO₂ photocatalysis; design and applications, *J. Photochem. Photobiol. C: Photochem. Rev.* 3 (2012) 169–189.
- [21] S. Malato, P. Fernández-Ibáñez, M.J. Maldonado, J. Blanco, W. Gernjak, Decontamination and disinfection of water by solar photocatalysis: Recent overview and trends, *Catal. Today* 147 (2009) 1–59.
- [22] M.N. Chong, B. Jin, C.W.K. Chow, C. Saint, Recent developments in photocatalytic water treatment technology: A review, *Water Res.* 44 (2010) 2997–3027.
- [23] M. Pelaez, N.T. Nolan, S.C. Pillai, M.K. Seery, P. Falaras, A.G. Kontos, P.S.M. Dunlop, J.W.J. Hamilton, J.A. Byrne, K. O'Shea, M.H. Entezari, D.D. Dionysiou, A review on the visible light active titanium dioxide photocatalysts for environmental applications, *Appl. Catal. B: Environ.* 125 (2012) 331–349.
- [24] L.M. Pastrana-Martínez, S. Morales-Torres, V. Likodimos, J.L. Figueiredo, J.L. Faria, P. Falaras, A.M.T. Silva, Advanced nanostructured photocatalysts based on reduced graphene oxide-TiO₂ composites for degradation of diphenhydramine pharmaceutical and methyl orange dye, *Appl. Catal. B: Environ.* 123–124 (2012) 241–256.
- [25] B. Neppolian, H. Choi, S. Sakthivel, B. Arabindoo, V. Murugesan, Solar/UV-induced photocatalytic degradation of three commercial textile dyes, *J. Hazard. Mater.* 2–3 (2002) 303–317.
- [26] V.K. Gupta, R. Jain, A. Mittal, T.A. Saleh, A. Nayak, S. Agarwal, S. Sikarwat, Photo-catalytic degradation of toxic dye amaranth on TiO₂/UV in aqueous suspensions, *Mater. Sci. Eng. C.* 32 (2012) 1–12.
- [27] W. Chu, Y.R. Wang, H.F. Leung, Synergy of sulfate and hydroxyl radicals in UV/S₂O₈²⁻/H₂O₂ oxidation of iodinated X-ray contrast medium iopromide, *Chem. Eng. J.* 178 (2011) 154–160.
- [28] J. Saien, Z. Ojaghloo, A.R. Soleymani, M.H. Rasoulifard, Homogeneous and heterogeneous AOPs for rapid degradation of Triton X-100 in aqueous media via UV light, nano titania hydrogen peroxide and potassium persulfate, *Chem. Eng. J.* 167 (2011) 172–182.
- [29] V. Augugliaro, M. Litter, L. Palmisano, J. Soria, The combination of heterogeneous photocatalysis with chemical and physical operations: A tool for improving the photoprocess performance, *J. Photochem. Photobiol. C: Photochem. Rev.* 7 (2006) 127–144.

- [30] S. Navalon, M. Alvaro, H. Garcia, Heterogeneous Fenton catalysts based on clays, silicas and zeolites, *Appl. Catal. B: Environ.* 99 (2010) 1–26.
- [31] J. Herney-Ramirez, M.A. Vicente, L.M. Madeira, Heterogeneous photo-Fenton oxidation with pillared clay-based catalysts for wastewater treatment: A review, *Appl. Catal. B: Environ.* 98 (2010) 10–26.
- [32] P.R. Gogate, A.B. Pandit, A review of imperative technologies for wastewater treatment II: hybrid methods, *Adv. Environ. Res.* 8 (2004) 553–597.
- [33] N. Quici, M.E. Morgada, G. Piperata, P. Babay, R.T. Gettar, M.I. Litter, Oxalic acid destruction at high concentrations by combined heterogeneous photocatalysis and photo-Fenton processes, *Catal. Today* 101 (2005) 253–260.
- [34] B. Tryba, M. Piszcz, B. Grzmil, A. Pattek-Janczyk, A.W. Morawski, Photodecomposition of dyes on Fe–C–TiO₂ photocatalysts under UV radiation supported by photo-Fenton process, *J. Hazard. Mater.* 162 (2009) 111–119.
- [35] R.A. Torres-Palma, J.I. Nieto, E. Combet, C. Pétrier, C. Pulgarin, An innovative ultrasound, Fe²⁺ and TiO₂ photoassisted process for bisphenol a mineralization, *Water Res.* 44 (2010) 2245–2252.
- [36] M. Zarei, A.R. Khataee, R. Ordikhani-Seyedlar, M. Fathinia, Photoelectro-Fenton combined with photocatalytic process for degradation of an azo dye using supported TiO₂ nanoparticles and carbon nanotube cathode: Neural network modeling, *Electrochim. Acta* 55 (2010) 7259–7265.
- [37] H. Feng, M.C.H. Zhang, L.E. Yu, Hydrothermal synthesis and photocatalytic performance of metal-ions doped TiO₂, *Appl. Catal. A: Gen.* 413–414 (2012) 238–244.
- [38] M. Khatamian, S. Hashemian, A. Yavari, M. Saket, Preparation of metal ion (Fe³⁺ and Ni²⁺) doped TiO₂ nanoparticles supported on ZSM-5 zeolite and investigation of its photocatalytic activity, *Mater. Sci. Eng. B* 177 (2012) 1623–1627.
- [39] L.G. Devi, B.N. Murthy, S.G. Kumar, Photocatalytic activity of TiO₂ doped with Zn²⁺ and V⁵⁺ transition metal ions: Influence of crystallite size and dopant electronic configuration on photocatalytic activity, *Mater. Sci. Eng. B* 166 (2010) 1–6.
- [40] L. Gu, Z. Chen, C. Sun, B. Wei, X. Yu, Photocatalytic degradation of 2,4-dichlorophenol using granular activated carbon supported TiO₂, *Desalination* 263 (2010) 107–112.
- [41] Z.H. Zhang, Y. Shan, J. Wang, H. Ling, S. Zang, W. Gao, Z. Zhao, H. Zhang, Investigation on the rapid degradation of congo red catalyzed by activated carbon powder under microwave irradiation, *J. Hazard. Mater.* 147 (2007) 325–333.
- [42] K. Yao, J. Gong, J. Zheng, L. Wang, H. Tan, G. Zhang, Y. Lin, H. Na, X. Chen, X. Wen, T. Tang, Catalytic carbonization of chlorinated poly(vinyl chloride) microfibers into carbon microfibers with high performance in the photodegradation of Congo Red, *J. Phys. Chem. C* 117 (2013) 17016–17023.
- [43] J. Molina, J.L. Sanchez-Salas, C. Zuniga, E. Mendoza, R. Cuahtecntzi, G. Garcia-Perez, E. Gutierrez, E.R. Bandala, Low-temperature processing of thin films based on rutile TiO₂ nanoparticles for UV photocatalysis and bacteria inactivation, *J. Mater. Sci.* 49 (2014) 786–793.
- [44] G.R.M. Echavia, F. Matzusawa, N. Negishi, Photocatalytic degradation of organophosphate and phosphonoglycine pesticides using TiO₂ immobilized on silica gel, *Chemosphere* 76 (2009) 595–600.
- [45] S. Fukahori, T. Fujiwara, Modeling of sulfonamide antibiotic removal by TiO₂/high-silica zeolite HSZ-385 composite, *J. Hazard. Mater.* 272 (2014) 1–9.
- [46] Z. Miao, S. Tao, Y. Wang, Y. Yu, C. Meng, Y. An, Hierarchically porous silica as an efficient catalyst carrier for high performance vis-light assisted Fenton degradation, *Microporous Mesoporous Mater.* 176 (2013) 178–185.
- [47] T. An, J. Chen, G. Li, X. Ding, G. Sheng, J. Fu, B. Mai, K.E. O'Shea, Characterization and the photocatalytic activity of TiO₂ immobilized hydrophobic montmorillonite photocatalysts. Degradation of decabromodiphenyl ether (BDE 209), *Catal. Today* 139 (2008) 69–76.
- [48] H. Bel Hadjltaief, P. Da Costa, M.E. Galvez, M. Ben Zina, Influence of operational parameters in the heterogeneous photo-Fenton discoloration of wastewaters in the presence of an iron-pillared clay. *Ind. Eng. Chem. Res.* 47 (2013) 16656–16665.
- [49] H. Bel Hadjltaief, P. Da Costa, P. Beaunier, M.E. Galvez, M. Ben Zina, Fe–clay-plate as a heterogeneous catalyst in photo-Fenton oxidation of phenol as probe molecule for water treatment, *Appl. Clay Sci.* 91 (2014) 46–54.
- [50] C. Bai, W. Xiao, D. Feng, M. Xian, D. Guo, Z. Ge, Y. Zhou, Efficient decolorization of Malachite Green in the Fenton reaction catalyzed by [Fe(III)-salen]Cl complex, *Chem. Eng. J.* 215–216 (2013) 227–234.
- [51] Y. Cao, Y. Hu, J. Sun, B. Hou, Explore various co-substrates for simultaneous electricity generation and Congo red degradation in air-cathode single-chamber microbial fuel cell, *Bioelectrochemistry* 79 (2010) 71–76.
- [52] G. Ivana, V. Dinko, K. Natalija, Modeling the mineralization and discoloration in colored systems by (US) Fe²⁺/H₂O₂/S₂O₈²⁻ processes: A proposed degradation pathway, *Chem. Eng. J.* 157 (2010) 35–44.
- [53] N.A. Ejhieh, B. Zohreh, Kinetic investigation of photocatalytic degradation of dimethyldisulfide by zeolite A containing nano CdS, *Iran. J. Catal.* 2 (2012) 77–81.
- [54] A. Nezamzadeh-Ejhieh, M. Karimi-Shamsabadi, Decolorization of a binary azo dyes mixture using CuO incorporated nanozeolite-X as a heterogeneous catalyst and solar irradiation, *Chem. Eng. J.* 228 (2013) 631–641.
- [55] M. Tekbaş, H. Yatmaz, N. Bektaş, Heterogeneous photo-Fenton oxidation of reactive azo dye solutions using iron exchanged zeolite as a catalyst, *Microporous Mesoporous Mater.* 115 (2008) 594–602.
- [56] J.Y. Feng, X.J. Hu, P.L. Yue, S.Z. Qiao, Photo Fenton degradation of high concentration orange II (2 mM) using catalysts containing Fe: A comparative study, *Sep. Purif. Technol.* 67 (2009) 213–217.
- [57] C. Catrinescu, C. Teodosiu, M. Macoveanu, J. Miehé-Brendlé, R. Le Dred, Catalytic wet peroxide oxidation of phenol over Fe-exchanged pillared beidellite, *Water Res.* 37 (2003) 1154–1160.
- [58] J.X. Chen, L.Z. Zhu, Catalytic degradation of Orange II by UV-Fenton with hydroxyl-Fe-pillared bentonite in water, *Chemosphere* 65 (2006) 1249–1255.
- [59] W. Najjar, S. Azabou, S. Sayadi, A. Ghorbel, Catalytic wet peroxide photo-oxidation of phenolic olive oil mill

- wastewater contaminants, *Appl. Catal. B: Environ.* 74 (2007) 11–18.
- [60] J. Feng, R.S.K. Wong, X. Hu, P.L. Yue, Discoloration and mineralization of orange II by using Fe³⁺-doped TiO₂ and bentonite clay-based Fe nanocatalysts, *Catal. Today* 98 (2004) 441–446.
- [61] M.A. De León, J. Castiglioni, J. Bussi, M. Sergio, Catalytic activity of an iron-pillared montmorillonitic clay mineral in heterogeneous photo-Fenton process, *Catal. Today* 133–135 (2008) 600–605.
- [62] Q. Chen, P. Wu, Z. Dang, N. Zhu, P. Li, J. Wu, X. Wang, Iron pillared vermiculite as a heterogeneous photo-Fenton catalyst for photocatalytic degradation of azo dye reactive brilliant orange X-GN, *Sep. Purif. Technol.* 3 (2010) 315–323.